Article

DFT and QTAIM analysis: Influence of intramolecular interactions on pirouetting movement in tetraalkylsuccinamide[2]rotaxanes

Marcos A. P. Martins, Leticia V. Rodrigues, Alexandre R. Meyer, Clarissa P. Frizzo, Manfredo Hörner, Nilo Zanatta, Helio G. Bonacorso, José Berná, and Mateo Alajarín

Cryst. Growth Des., **Just Accepted Manuscript** • DOI: 10.1021/acs.cgd.7b00944 • Publication Date (Web): 26 Sep 2017

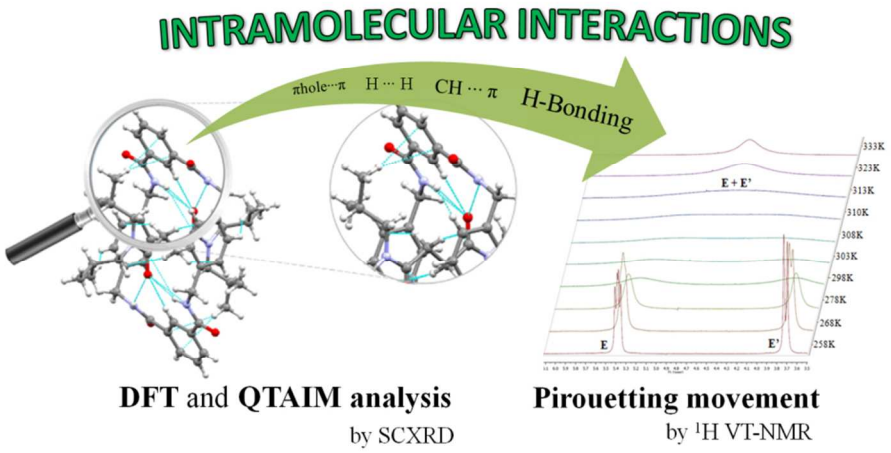

88x42mm (300 x 300 DPI)

DFT and QTAIM analysis: Influence of intramolecular interactions on pirouetting movement in tetraalkylsuccinamide[2]rotaxanes

Marcos A. P. Martins[†*], *Leticia V. Rodrigues*[†], *Alexandre R. Meyer*[†], *Clarissa P. Frizzo*[†], *Manfredo Hörner*[‡], *Nilo Zanatta*[†], *Helio G. Bonacorso*[†], *Jose Berná*[§], *and Mateo Alajarín*[§]

[†] Núcleo de Química de Heterociclos (NUQUIMHE), Departamento de Química, Universidade Federal de Santa Maria, 97105-900 Santa Maria, RS, Brazil.

[‡] Núcleo de Investigação de Triazenos (NITRICO), Departamento de Química, Universidade Federal de Santa Maria, 97105-900 Santa Maria, RS, Brazil.

[§] Departamento de Química Orgánica, Facultad de Química Regional Campus of International Excellence "Campus Mare Nostrum", Universidad de Murcia, E-30100 Murcia, Spain.

KEYWORDS: [2]rotaxanes, QTAIM analysis, intramolecular interactions, VT-NMR experiments, X-ray crystal.

ABSTRACT: The first Quantum Theory of Atoms in Molecules (QTAIM) analysis of [2]rotaxanes was used in combination with quantum mechanical calculations and VT-NMR experiments. The study shows all the intramolecular interactions of tetraalkylsuccinamide[2]rotaxanes with different templates. The threads have different stoppers [$R_1R_2NC(O)$-CH_2CH_2-$C(O)NR_2R_1$, in which R_2/R_1 = CH_2*cy*-Hex/CH_2Ph, *i*-Bu, Bu, and Pr]. The different threads used let us verify that the contact area between the submolecular components ($C_{Mcy\cdots Thr}$) is closely correlated with the interaction energy ($G_{Mcy\cdots Thr}$) in the [2]rotaxanes studied. Furthermore the QTAIM data and quantum mechanical calculations confirmed that, in all of the compounds, the hydrogen bonds are responsible for most of the energy from the intramolecular interactions that follow the C–H···π and H···H interactions, independent of the thread used. In the liquid state, using NMR ^{1}H some intramolecular interactions were observed, which is in agreement with the data obtained in the solid state, thus making possible a comparison between the energy data obtained via the quantum mechanical calculations and the molecular movements of the [2]rotaxanes in solution. Consequently, a new way of understanding the intramolecular interactions in [2]rotaxanes and the influence they have on the movement of molecular machines is presented.

Introduction

Mechanically interlocked architectures, such as catenanes and rotaxanes, offer very attractive access to intramolecular interactions, due to the submolecular components being connected by a mechanical bond, and the molecular interactions being present from the moment that their synthesis begins with the self-assembly of multi-components. [1–3] In particular, the rotaxanes consist of two or more submolecular components, with at least one macrocycle locked onto a

linear component (thread). In principle, the submolecular components can move relative to one another without breaking covalent bonds, and this fact makes these compounds similar to molecular machines.[4–6]

Recently, we showed: the dynamic behaviour of succinamide templates in the preparation of [2]rotaxanes containing benzylic amide macrocycle and cyclohexylmethyl substituents as stoppers, and how the stoppers cause interference in the pirouetting submolecular motion of these interlocked molecules.[7] Additionally, another study we show the relationship between the size of the components and the stability of the [2]rotaxanes, indicating the influence of the straight and branched alkyl stopper groups in the deslipping reactions. [8] In particular, in previous works we used techniques to demonstrate how the stopper can have an influence in the deslipping and the pirouetting movement. Considering that these submolecular movements are correlated to the intramolecular interactions, a complete study of these interactions is necessary. The large family of rotaxanes that is based on a thread containing a hydrogen-bonding template for the benzylic amide macrocycle has the shuttling and pirouetting movements well-established in solution, [9–12] but only once have these rotaxanes been studied in the solid state.[13] Soon these compounds have rarely been investigated in the literature within static quantum chemical calculations.[14,15]

Another attractive feature of Leigh-type [2]rotaxanes is that they are excellent molecules for the study of intramolecular interactions, due to them having donor and acceptor hydrogen-bond groups and π-electrons that allow various interactions involving π-systems; for example π···π, CH···π, πhole···π, and lone-pair···π interactions. In this sense, supramolecular chemistry has grown and been developed in recent years in an effort to explain how molecules interact with each other by intramolecular and intermolecular interactions; [16] however, there is a lack of

supramolecular studies of [2]rotaxanes in the literature. Literature works [17–21] have established only hydrogen bonding in [2]rotaxanes, via purely geometrical criteria that do not give due attention to the other intramolecular interactions existing in these compounds.

Consequently, Quantum Theory of Atoms in Molecules (QTAIM) is a useful tool for characterizing non-covalent interactions. [22–25] For the pair of atoms that are interacting, there is the bond path (BP) with the corresponding bond critical point (BCP), where the electron density (ρ_{BCP}) is established. Several studies have shown that the energy of an atom···atom interaction can be estimated from the electron density at the BCP. [25]

Thus, this present study was to demonstrate the existence of complementary regions between thread and macrocycle in [2]rotaxanes. In order to achieve this, the molecular electrostatic potential (MEP) and the correlation between the contact area of the thread-macrocycle and the interaction energy ($G_{Mcy\cdots Thr}$) were used. In this paper, our main objective was to quantitatively and qualitatively establish all the intramolecular interactions — via QTAIM and calculations using density functional theory (DFT) — in the compounds studied. The ^{1}H NMR experiments were used in order to compare the interactions in the solid state with those in the liquid state, thereby correlating the energy of the pirouetting in the compounds studied and showing how the intramolecular interactions can affect the movement of molecular machines.

Experimental Section

General: All reagents and solvents were commercially available and were used without further purification. Column chromatography was carried out using silica gel (60 Å, 40-60 μm, SDS) as stationary phase, and TLC was carried out using silica gel on aluminun cards (0.25 mm thick, with fluorescent indicator 254 nm, Fluka) and observed under UV light. The ^{1}H and ^{13}C NMR spectroscopic data were recorded with a Bruker AVANCE 400 (^{1}H NMR at 400.13 MHz and ^{13}C

NMR at 100.62 MHz) in $CDCl_3$/TMS solutions, and the VT-NMR experiments were recorded with a Bruker DPX 400 (^{1}H NMR at 400.13 MHz and ^{13}C NMR at 100.62 MHz) or AVANCE 600 (^{1}H NMR at 600.13 MHz and ^{13}C NMR at 150.62 MHz), in $CDCl_3$/TMS or $C_2D_2Cl_4$/TMS solutions. The chemical shifts (δ values) are given in ppm. Signals in the ^{1}H and ^{13}C NMR spectra of the synthesized compounds were assigned with the aid of two-dimensional NMR experiments (COSY, HMBC, NOESY and HMQC). Analyses exact mass of the [2]rotaxane was performed on a mass spectrometer HP HPLC / MS 6220 TOF with direct insertion mode electrosprey positive.

Materials and Methods: To prepare the [2]–[*N*,*N*'-bisbenzyl-*N*,*N*'-bisciclohexylmetylsuccinamide]– rotaxa–[1,7,14,20-tetraaza-2,6,15,19- tetraoxo-3,5,9,12,16,18,22,25-tetrabenzocicloexacosano] (compound 4) the reaction steps described below are required.

N-(ciclohexylmetyl)(fenyl)metanamine: The mixture of benzylamine (1.96 mL, 18 mmol) , cyclohexane carboxaldehyde (2.18 mL, 18 mmol) and CH_2Cl_2 (40 mL) was added to a flask and was subsequently added sodium triacetoxyborohydride (5.70 g, 27 mmol) . The mixture was stirred at 25 ° C for 4 h under N_2 atmosphere. After completion of the reaction time was added slowly a saturated solution of $NaHCO_3$ (30 mL) and the resulting mixture was stirred at 25 ° C for 30 minutes . The resulting mixture was extracted with ethyl acetate and the organic phase was washed with saturated NaCl solution (3 × 30 ml) . Then , the organic phase was dried with anhydrous sodium sulfate (Na_2SO_4), filtered and the solvent was evaporated under reduced pressure. The product was purified by column chromatography, using hexane/ethyl acetate (98:2) as eluent. The product was obtained with 84 % yield. ^{1}H-NMR (400 MHz, $CDCl_3$): δ , J_{HH} (Hz):

0.83-1.79 (m, 11H); 2.48 (d, ^3J =7, 2H); 3.79 (s, 2H); 7.73 (s, 5H). The compound has been characterized in the literature.[26–28]

N,*N*'-bisbenzyl-*N*,*N*'-bisciclohexylmetylsuccinamide: To a solution of the *N*-(ciclohexylmetyl)(fenyl)metanamine (8 mmol), triethylamine (8 mmol) in CH_2Cl_2 (50 mL), succinyl dichloride (4 mmol) in CH_2Cl_2 (10 mL) was added droppwise at 0ºC. The reaction mixture was stirred for 20 hours at room temperature under N_2 atmosphere. After this time the solution was washed with NaOH 1M (2 × 30mL), HCl 1M (2 × 30 mL) and brine (2 × 30 mL). The organic phase was dried over anhydrous $MgSO_4$ and concentrated under reduced pressure. The residue was subjected to column chromatography on silica gel using using $CHCl_3$/MeOH (95:5) as eluent to give the corresponding thread. The product was obtained with 85 % yield. ^{1}H-NMR (400 MHz, $CDCl_3$): δ 0.95-1.28 (m,11H); 1.68 (brs, 11H); 2.76 (d,^2J = 16, 4H); 3.24 (dd, ^2J = 13, ^3J = 7, 4H,); 4.62 (s, 4H); 7.23 (m, 10 H). / 0.95-1.28 (m,11H); 1.68 (brs, 11H); 2.75 (d, ^2J = 16, 4H); 3.14 (dd, ^2J = 12, ^3J = 7, 4H,); 4.65 (s, 4H); 7.23 (m, 10 H). ^{13}CNMR (100 MHz, $CDCl_3$): δ 25.; 26.3; 28.6; 29.6; 36.4; 49; 53.2; 127; 127.7; 128.7; 137.8; 172.5; 172.7. / 25.9; 26.4; 28.8; 30.96; 37.1; 52.3; 52.4; 126.6; 127.2; 128.4; 137.2; 172.6; 172.8. LCMS-MS [$(M+H)^+$, 489]

[2]–[*N*,*N*'-bisbenzyl-*N*,*N*'-bisciclohexylmetylsuccinamide]– rotaxa–[1,7,14,20-tetraaza-2,6,15,19- tetraoxo-3,5,9,12,16,18,22,25- tetrabenzocicloexacosane]: The thread was solubilized in anhydrous chloroform (300 mL) in the presence of triethylamine (24 mmol). Stirred vigorously whilst solutions of *p*-xylylenediamine (8 mmol), in anhydrous chloroform (20 mL) and the isophthaloyl dichloride (8 mmol) in anhydrous chloroform (20 mL) were simultaneously added over a period of 4 h using motor-driven syringe pumps. After a further 4 h the resulting suspension was filtered through a Celite and the solvent removed under reduced pressure. The

resulting solid was subjected to column cromatography (silica gel) using $CHCl_3$/MeOH (99:1) mixture as eluent to give the [2]rotaxanes. The product was obtained with 28 % yield. ^{1}H-NMR (400 MHz, $CDCl_3$): δ0.22-0.96 (m, 11H); 1.05 (s, 4H); 1.07-1.47 (m, 11H); 2.80 (d, ^3J = 7, 4H); 4.39 (s, 4H,); 6.88 (s, 10H); 7.33 (s, 8H); 7.49 (t, ^3J = 6, 4H); 7.68 (t, ^3J = 7 2H); 8.40 (d, J = 8, 2H,); 8.78 (s, 2H)./ 0.22-0.96 (m, 11H); 1.07-1.47 (m, 11H); 1.78 (s, 4H); 2.76 (d,^3J = 7, 2H); 3.37 (d,^3J = 7, 2H); 4.10 (s, 2H); 4.29 (s, 2H); 6.75 (s, 5H); 6.73 (s, 5H); 7.17 (t, ^3J = 7, 4H); 7.29 (s, 8H), 7.64 (t, ^3J = 7, 2H); 8.37 (d, ^3J = 8, 2H); 8.65 (s, 2H)./ 0.22-0.96 (m, 11H); 1.07-1.47 (m, 11H); 1.26 (s, 4H); 3.25 (d, ^3J = 6, 4H); 4.06 (s, 4H,); 6.88 (s, 10H); 7.03 (t, 4H); 7.33 (s, 8H); 7.61 (t, ^3J = 8, 4H); 8.30 (d, ^3J = 8, 2H); 8.47 (s, 2H). ^{13}CNMR (100 MHz, $CDCl_3$): δ 25.3; 31.3; 36.3; 42.8; 51.1; 55.1; 122; 125.5; 128.4; 129.9; 132.2; 133.2; 135.5; 138.1; 165,0; 173,3./25.3; 31.3; 36.4; 43.2; 52.6; 52.7; 55.5; 56.0; 122.4; 128.1; 128.4; 129.9; 132.4; 133.3; 136.8; 138.3; 165.2; 173.5. / 25.3; 31.3; 37.4; 43.5; 54.2; 54.7; 122.5; 128.2; 128.4; 129.9; 132.5; 133.4; 136.9; 138.5; 165.5; 174.5. HRMS (ESI) calcd for $C_{64}H_{72}N_6O_6$ [M + H]+ 1020,5518, found 1021,5618.

The spectra of the synthesized compounds are given in Supportin Information Figure S1-S5.

Crystallographic data collection and structure determination: The diffraction measurements of compound 1 was carried out by graphite monochromatized Mo Kα radiation with λ = 0.71073 Å on a Bruker D8 VENTURE diffractometer with a goniometer KAPPA four circles, equipped with PHOTON II CPAD area detector, at 100 K. The compounds 2-4 were carried out by graphite monochromatized Mo Kα radiation with λ = 0.71073 Å on a Bruker SMART CCD diffractometer.[29] The structures were solved with direct methods using the SHELXS program, and refined on F2 by full-matrix least-squares with the SHELXL package.[30] Absorption correction was performed by the Gaussian method.[31] Anisotropic displacement parameters for

non-hydrogen atoms were applied. The hydrogen atoms were placed at calculated positions with 0.96 (methyl CH_3), 0.97 (methylene CH_2), 0.98 (methyne CH), 0.93 (aromatic CH), and 0.82 Å (OH) using a riding model. Hydrogen isotropic thermal parameters were kept equal to Uiso(H) = xUeq (carrier C atom), with x = 1.5 for methyl groups and x = 1.2 otherwise. The valence angles C–C–H and H–C–H of methyl groups were set to 109.5°, and H atoms were allowed to rotate around the C–C bond. Graphic projections were constructed using Ortep3 for Windows program included in WinGx program package.[32] Parameters in CIF format are available as an electronic supplementary publication from the Cambridge Crystallographic Data Centre (CCDC 1539700 (1), 1542403 (2) and 1550499 (3) 1539696 (4)). The crystal data and details concerning data collection and structure refinement are given in Table 1. The micrographics of the compounds 1-4 given in Supportin Information Figure S6.

Table 1. Data collection and structure refinement for structure of **1-4**.

Compound	**1**	**2**	**3**	**4**
CCDC Number	1539700	1542403	1550499	1539696
Empirical formula	$C_{32}H_{36}N_3O_3$	$C_{26}H_{34}N_3O_3$	$C_{52}H_{68}N_6O_6$	$C_{26}H_{28}Cl_4N_3O_3$
Formula weight	510.64	436.56	873.12	572.31
Temperature (K)	293(2)	296(3)	293(2)	293(2)
Wavelenght (Å)	0.71073	0.71073	0.71073	0.71073
Crystal system	Triclinic	Triclinic	Triclinic	Triclinic
Space group	$P\ 1\ -$	$P\ 1\ -$	$P\ 1\ -$	$P\ 1\ -$
a (Å)	10.065 (5)	10.3051(6)	12.3496(10)	10.0010(3)
b (Å)	11.064(5)	11.0239(7)	13.1703 (11)	11.6711(4)
c (Å)	12.664(5)	11.6493(8)	15.7235(13)	13.1113(4)

α (deg)	103.731(5)	80.705(4)	85.736(5)	76.249(2)
β (deg)	98.250(5)	67.383(4)	82.630(5)	73.972(2)
γ (deg)	92.239(5)	77.728(4)	73.470(5)	83.515(2)
Volume ($Å^3$)	1351.8(11)	1189.02(13)	2429.5	1426.90(8)
Z/density (calcd)(Mg/m^3)	2, 1.254	2, 1.219	2, 1.194	2, 1.332
Absorption coefficient (mm^{-1})	0.081	0.080	0.078	0.446
F(000) (e)	546.0	470	940	594
Crystal size (mm^3)	0.41 × 0.36 × 0.18	0.22 × 0.17 × 0.12	0.548 × 0.348 × 0.186	0.582 × 0.474 × 0.204
θ range of data collection (deg)	2.20 to 30.10	1.90 to 26.91	1.31 to 26.91	1.80 to 27.16
Reflections collected/unique	53309 / 7901 [R(int) = 0.027	32265 / 5067 [R(int) = 0.0755]	68942 / 10372 [R(int) = 0.0736]	39993 / 6281 [R(int) = 0.0402]
Completeness to θ (%)	(30.10) 99.1 %	(26.91) 98.5%	(26.91) 98.7%	(27.16) 99.4%
Absorption correction	Gaussian	Gaussian	Gaussian	Gaussian
Max. and min. transmission	0.9906 and 0.9616	0.9904 and 0.9826	0.99937 and 0.99830	0.928 and 0.793
Refinement method	Full-matrix least-squares on F^2	Full-matrix least-squares on F^2	Full-matrix least-squares on F^2	Full-matrix least-squares on F^2
Data/restraints/parameters	7901 / 0 / 343	5067 / 4 / 288	10372 / 0 / 578	6281 / 0 / 316
Goodness-of-fit on F^2	1.038	0.996	0.958	1.065
Final R indices [$I \geq 2\sigma(I)$][a]	R_1 = 0.0619, wR_2 = 0.1509	R1 = 0.0527, wR2 = 0.1180	R1 = 0.0720, wR2 = 0.1977	R_1 = 0.0820, wR_2 = 0.2369
R_1 (all data)[a]	R_1 = 0.0744, wR_2 = 0.1613	R1 = 0.1334, wR2 = 0.1494	R1 = 0.2330, wR2 = 0.2831	R_1 = 0.1312, wR_2 = 0.2769
Larges diff. peak and hole (e A^{-3})	0.973 and -0.570	0.162 and -0.174	0.295 and -0.205	1.446 and -0.517

Computational Computational Details: All quantum mechanical calculations were performed with the aid of the Gaussian© 09 software package.[33] To obtain the interaction energy between thread and macrocycle Density Functional Theory (DFT) with the level of theory ωB97XD/cc-pVDZ was used. The counterpoise method of Boys and Bernardi [34] was employed to minimize the error of overlapping bases (BSSE). Dihedral amide angle of the compound (**1**) were changed from 0 to 360° in steps of 10° optimizing the geometry at the PM6 level. The geometry of the most stable conformers was fully re-optimized without any constrain at the ωB97X-D/cc-pVDZ level of theory. All geometries were verified as minima on the potential energy by calculating the Hessian matrices by harmonic frequency calculations. The atomic coordinates used in theoretical calculations are given in Supporting Information **Table S1**.

Quantum Theory of Atoms In Molecules (QTAIM) Data: All QTAIM analyses were performed with the aid of the AIMALL program package.[35] The wave functions used in the QTAIM analyses were generated at the ωB97XD/cc-pVDZ level of theory. The bond paths show which atoms are interacting and the analyses of the electron density at the BCP provide important information about the intramolecular interactions. The electron density (ρ) value at the BCP is related to the intermolecular interaction strength; the greater the ρ value, the greater the interaction energy. The Laplacian of the electron density ($\nabla^2\rho$) shows the nature of the interaction. Positive $\nabla^2\rho$ values indicate that the interaction is electrostatic in nature (ionic interactions, hydrogen bonds and halogen bonds), while negative Laplacian values indicate that the interaction is covalent in nature. [23,24] The QTAIM data and details concerning data collection and structure refinement are given in Supporting Information Table S2-S6.

Molecular Electrostatic Potential (MEP): Considering the electrostatic nature of the interactions, the electrostatic potential in compounds **1-4** is distributed along the molecular

regions of high and low molecular electrostatic potential (MEP)—the red areas indicate that the MEP is negative while the blue ones indicate that it is positive.[36] The Electrostatic Potential Maps were generated with a value of 0.001 a.u. of isodensity surface with The GaussView® [33] program from wave functions generated at the theory level ωB97XD/cc-pVDZ. These calculations were made from geometries obtained by X-ray diffractometry without single-point optimization.

Voronoi–Dirichlet polyhedron (VDP): The contact area between the thread and the macrocycle were constructed and TOPOS® version 4.0 software, [37] were taken directly from the CIF file generated by X-ray diffraction. The molecular Voronoi–Dirichlet polyhedron (VDP) concept was introduced in order to find the contact between the thread and macrocycle. This introduced the idea of the face of the one subcomponent molecular as a set of atomic VDP faces corresponding to the adjacent contacts between the atoms of the other subcomponent molecular. The datas obtained by TOPOS® are given in Supporting Information Table S7.

NCI analysis: The NCIPLOT program [38] was used to identify and visualize non-covalent interaction. As input of the program were used the wave functions generated at the ωB97X-D/cc-pVDZ level of theory. Reduced density gradient isosurfaces have been generated with NCIPLOT program and visualized with VMD [39]. A density cut-off of 0.1 a.u was applied and NCI figures have been generated with an isosurface of 0.4 and color scale of $-0.02 < \rho < 0.02$ a.u.

Results and Discussion

We chose four compounds for this work, in order to study the intramolecular interactions in [2]rotaxanes. All of the rotaxane tetralactam macrocycles in this report are comprised of two 1,4-phenylene side-walls that are connected by two identical isophthalamide units. The threads have

a succinamide station and different stoppers (e.g., CH_2*cy*-Hex/CH_2Ph, *i*-Bu, Bu, or Pr — see Figure 1). The [2]rotaxanes **2–4** — which have symmetrical stoppers and were completely characterized in a previous work [8] — were prepared by the clipping method. The [2]rotaxane **1** has a thread with unsymmetrical stoppers (CH_2*cy*-Hex and CH_2Ph), and it is described for the first time here (see Experimental Sections and Supporting Information for full details).

It is worth mentioning that unsymmetrical amides typically fluctuate between different conformational forms through the rotation of C(O)-N covalent bonds. Thus, for compound **1**, three different conformers were identified in solution (Figure 2), for which the following percentages of unsymmetrical amides were detected by integrating the ^{1}H NMR signal: 72% for conformer **1a** (*Z*-*Z*), 22% for conformer **1b** (*Z*-*E*), and 6% for conformer **1c** (*E*-*E*).

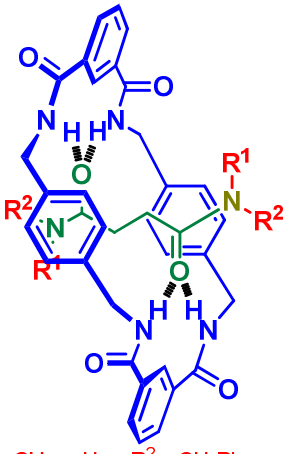

(1) R^1 = CH_2*cy*-Hex, R^2 = CH_2Ph,
(2) R^1 = R^2 = *i*-Bu,
(3) R^1 = R^2 = Bu,
(4) R^1 = R^2 = Pr.

Figure 1. Structures of compounds **1–4** used in this study.

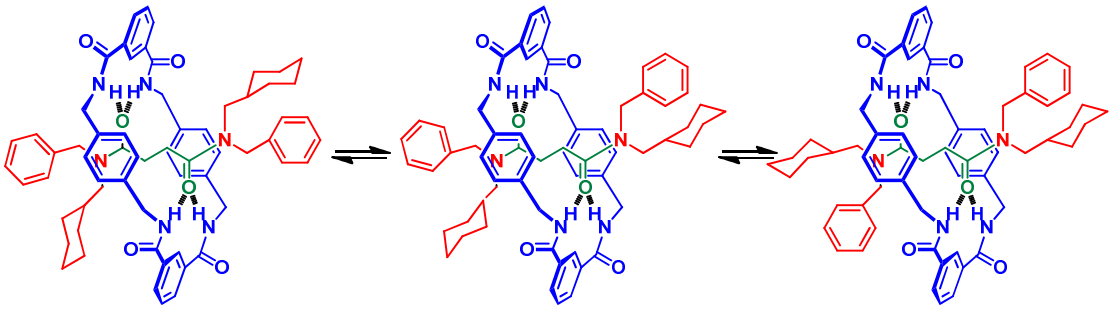

Figure 2. Conformers identified for compound **1**.

Compounds **1–4** were firstly crystallized and their structures were subsequently determined by X-ray diffraction (Figure 3). The crystals were obtained by slow evaporation of a solvent or a mixture of solvents: a mixture of chloroform and methanol (1:1) for compound **1**; only chloroform for compounds **2** and **3**; and tetrachloroethane (1:1) for compound **4**. The X-ray structure showed a number of notable features: (*i*) all the compounds have the macrocycle in a chair conformation that is commonly observed with Leigh-type rotaxanes; [40–43] (*ii*) the chair macrocycles are located centrally and symmetrically over the succinamide station, which suggests two possible sets of bifurcated hydrogen bonds between the amide groups of the macrocycle and the carbonyl groups of the succinamide system; [44,45] (*iii*) there is spatial proximity between the anti-alkyl chain group of the stoppers and the isophthalamide unit of the macrocycle, which suggests the existence of CH···π intramolecular interaction; [7] (*iv*) from the three different tertiary amide conformers present in solution for compound **1** (see Figure 2), only conformer **1a** is found in the crystal; (*v*) due to small differences in the conformation of the alkyl chain of the stoppers (see red circle in Figure 3), compound **3** crystallized with two independent molecules in the asymmetric unit, which is why the intramolecular interactions for the two molecules will be studied (compounds **3a** and **3b**); and (*vi*) the [2]rotaxane **4** crystallized with a

solvent molecule in the asymmetric unit, but this will not spoil this study, because in this work we are only interested in intramolecular interactions between the thread and the macrocycle.

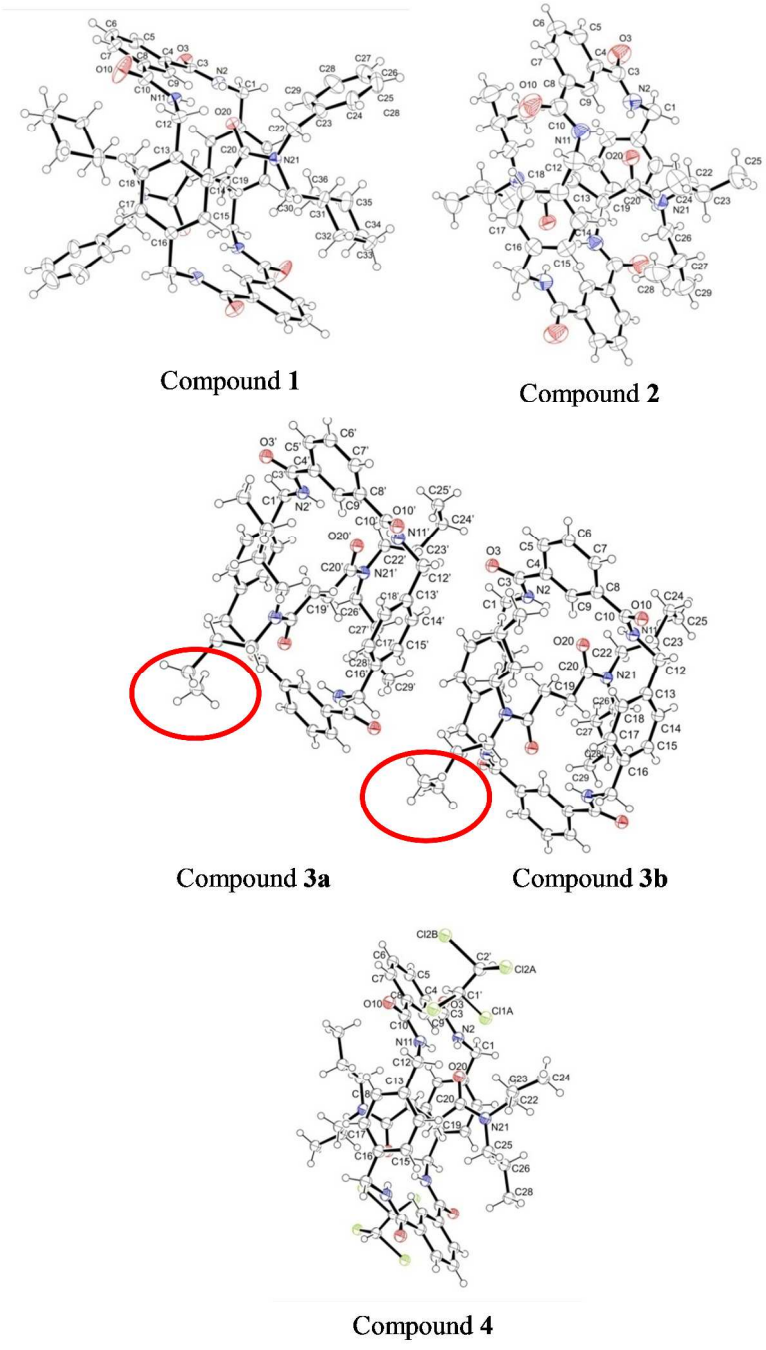

Figure 3. Molecular structures of compounds **1–4** represented by ORTEP® diagrams, with thermal ellipsoids drawn at the 50% probability level.

Additionally, single-point calculations were performed in order to determine the interaction energies ($G_{Mcy\cdots Thr}$) between thread and macrocycle for all compounds, using DFT at the ωB97X-D/cc-pVDZ level of theory with BSSE correction. The contact area between thread and macrocycle ($C_{Mcy\cdots Thr}$) for compounds **1–4** was also determined in order to correlate with the interaction energies ($G_{Mcy\cdots Thr}$). Data regarding the contact area ($C_{Mcy\cdots Thr}$) — which were obtained using TOPOS® [37] — and the interaction energies ($G_{Mcy\cdots Thr}$) for compounds **1—4** are shown in Table 2. It was possible to establish that the increase in the interaction energies is closely related to the increase in the size of the stoppers, and the consequent increase in the contact area is due to the greater possibility of intramolecular interactions between stoppers and macrocycles. Thus, we found a good correlation between the $G_{Mcy\cdots Thr}$ and $C_{Mcy\cdots Thr}$ data ($C_{Mcy\cdots Thr}$ = -4.9 $G_{Mcy\cdots Thr}$ = - 80.6; r = 0.942 — see Figure S13 in Supporting Information). In previous works [46] we showed that when the compounds present classical hydrogen bonds, there is no good correlation between the contact area and energy; however, this fact is diluted in all compounds, because all the compounds of the series studied have strong hydrogen bonds.

Table 2. Interaction energies and contact surfaces for compounds **1**–**4**.

Cpd	$G_{Mcy\cdots Thr}$ [a]	$C_{Mcy\cdots Thr}$ [b]
1	-58.31	204.62
2	-52.84	187.02
3a	-52.87	178.26
3b	-52.06	173.57
4	-51.65	168.69

[a] In kcal mol $^{-1}$, determined using the equation $G_{Mcy\cdots Thr} = E_{Rotax} - (E_{Thr} + E_{Mcy})$

[b] In Å^2, determined using TOPOS®

Accordingly, the MEP of compounds **1–4** is a useful tool for analysing complementary regions between zones with negative and positive potentials, and suggesting how the molecules interact with one other. In the study of the intramolecular interactions, it is more valid to generate the MEP for the thread and the macrocycle separately. Through analysis of the MEP we found a common pattern in all of the compounds, which demonstrates the negative electrostatic potential in the carbonyl oxygens atoms (red, in the thread) and the positive electrostatic potential in the nitrogens of the amides (blue, in the macrocycle). This electrostatic complementarity confirms that the Leigh-type [2]rotaxanes are formed by hydrogen bonds formed between the NH (macrocycle) and the O (thread) — see Figure 4. On the other hand, Figure 5 shows the MEP for compound **1**, with an isosurface value of 0.01 — when observing the two isosurfaces at the same time in this figure, it is possible to see that the thread is interpenetrated in the macrocycle.

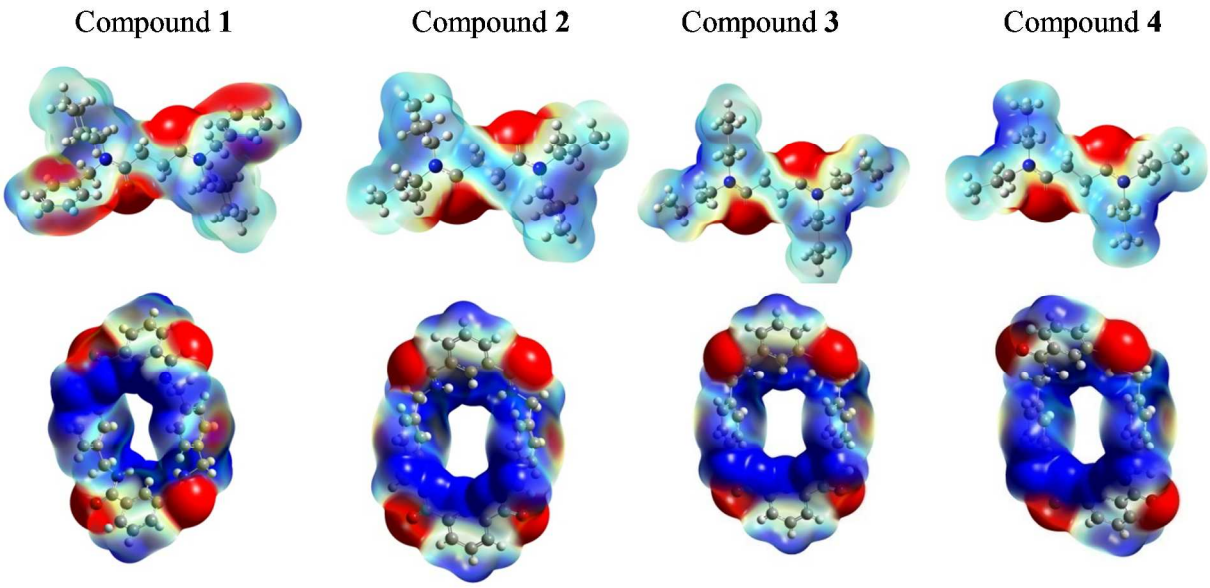

Figure 4. View of the MEPs of the thread and macrocycle for compounds **1**–**4**, obtained with an isodensity value of 0.001 (red = -0.02 a.u., yellow = -0.01 a.u., green = 0.00 a.u., and blue = 0.02 a.u.).

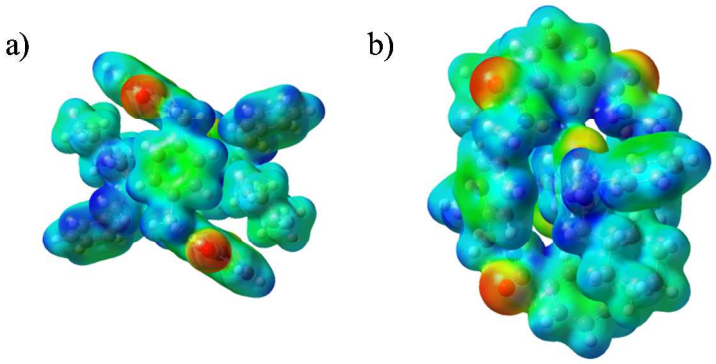

Figure 5. View of the MEP of rotaxane 1 with an isodensity value of 0.01 (red = -0.02 a.u., yellow = -0.01 a.u., green = 0.00 a.u., and blue = 0.02 a.u): a) side view of the chair macrocycle in the [2]rotaxane 1; and b) internal view of the chair macrocycle in the [2]rotaxane 1.

In order to identify all intramolecular interactions and understand how they affect the G_{int} of each molecule, calculations based on QTAIM were performed with the aid of the AIMAL® program. From the QTAIM analysis, the presence of the intramolecular interaction is given by a BCP along the bond path connecting two interacting atoms. [22,46,47] The results are shown in Table S2-S6 (see Supporting Information) — the threads and macrocycle showed bond paths, which confirms the interlocked nature of the molecules, and the number of interaction paths increased proportionately with the volume of the stoppers (Figure 6), thus corroborating the data discussed in Table 2. Another important observation is that all the [2]rotaxanes studied are symmetric molecules, so the interactions appear in pairs, thus confirming the perfect symmetry of the molecule.

In previous works [46–48] we showed a good correlation between the sum of the electron density ($\sum\rho_{INT}$) at the BCP and the interaction energy. In other words, the energy contribution of atom···atom interactions is proportional to the ρ_{INT}, which allows the portioning of the energy into

atom···atom interactions so that we can derive the energy value for the intramolecular interaction (G_{AI}). The types of atom···atom interactions and energy values of the intramolecular interactions (G_{AI}) of all the compounds are listed in Supporting Information. The ρ_{INT} values used in the determination of the G_{AI} of each intramolecular interaction are given in the Supporting Information.

Based on the literature, it is known that hydrogen bonds are the most important interactions for the formation of Leigh-type amide [2]rotaxanes, [45,49–51] because they are the ones that drive the formation of the mechanically interlocked molecules. Although QTAIM analysis has never been done before on [2]rotaxanes, it confirms the importance of the hydrogen bonds in these compounds. This is evident when we observe Figure 7, which shows the energy contribution (in percentage) and how much each type of interaction contributed to the total energy of the intramolecular interactions. Additionally, other important contributions like CH···π, H···H, and π_{hole}···π interactions were observed.

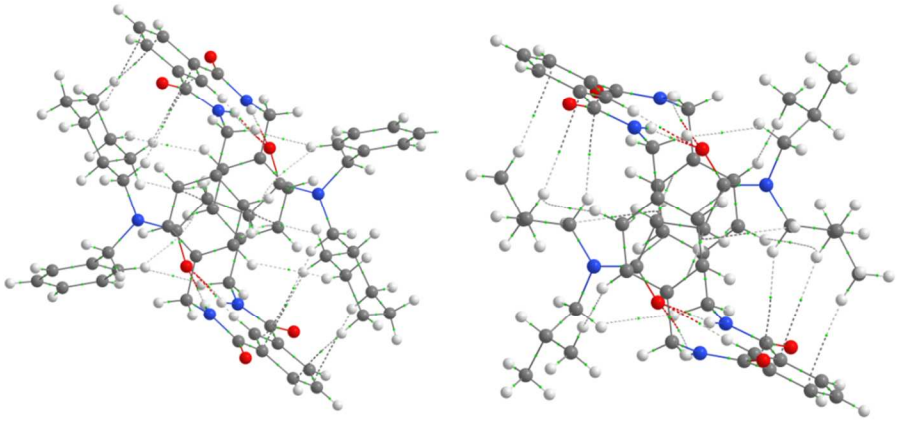

Compound **1**

Compound **2**

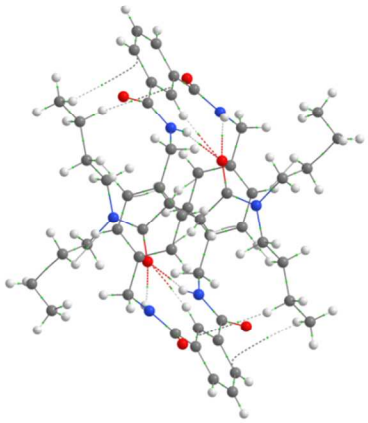

Compound **3a**

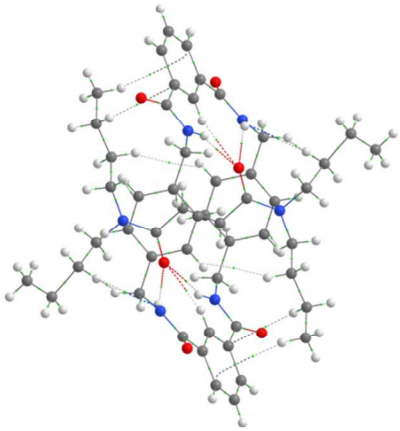

Compound **3b**

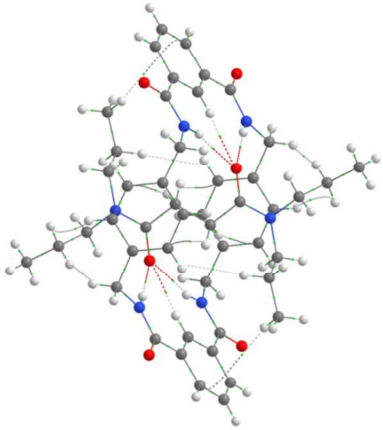

Compound **4**

Figure 6. View of the intramolecular interactions with the BCP's connecting interacting atoms.

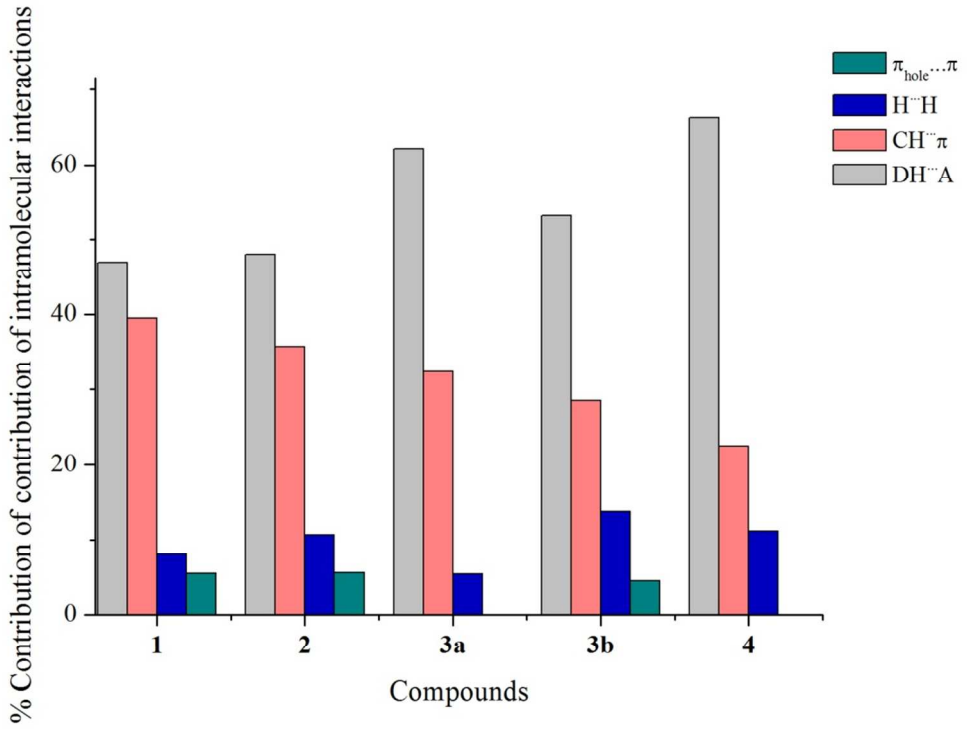

Figure 7. Energetic contribution (in percentage) of Thr···Mcy intramolecular interactions in compounds **1–4**, obtained from the fragmentation of QTAIM.

The QTAIM analysis (Table S2-S6 and Figure 7) showed that in all of the compounds, most of the atom···atom interaction energies (G_{AI}) are related to the hydrogen bonds between the carbonyl of the thread and the macrocycle. These interactions can be classified as: (*i*) two sets of N-H···O interactions, between the NH of the macrocycle and the carbonyl oxygens of the thread (-3.22 to -6.42 kcal mol^{-1}, except for compound **2** with -1.76 kcal mol^{-1}); and (*ii*) a set of C-H···O interactions, between the CH belonging to the isophthalamide unit of the macrocycle and the carbonyl oxygens of the thread (-4.50 to -6.32 kcal mol^{-1}) — see Figure 8.

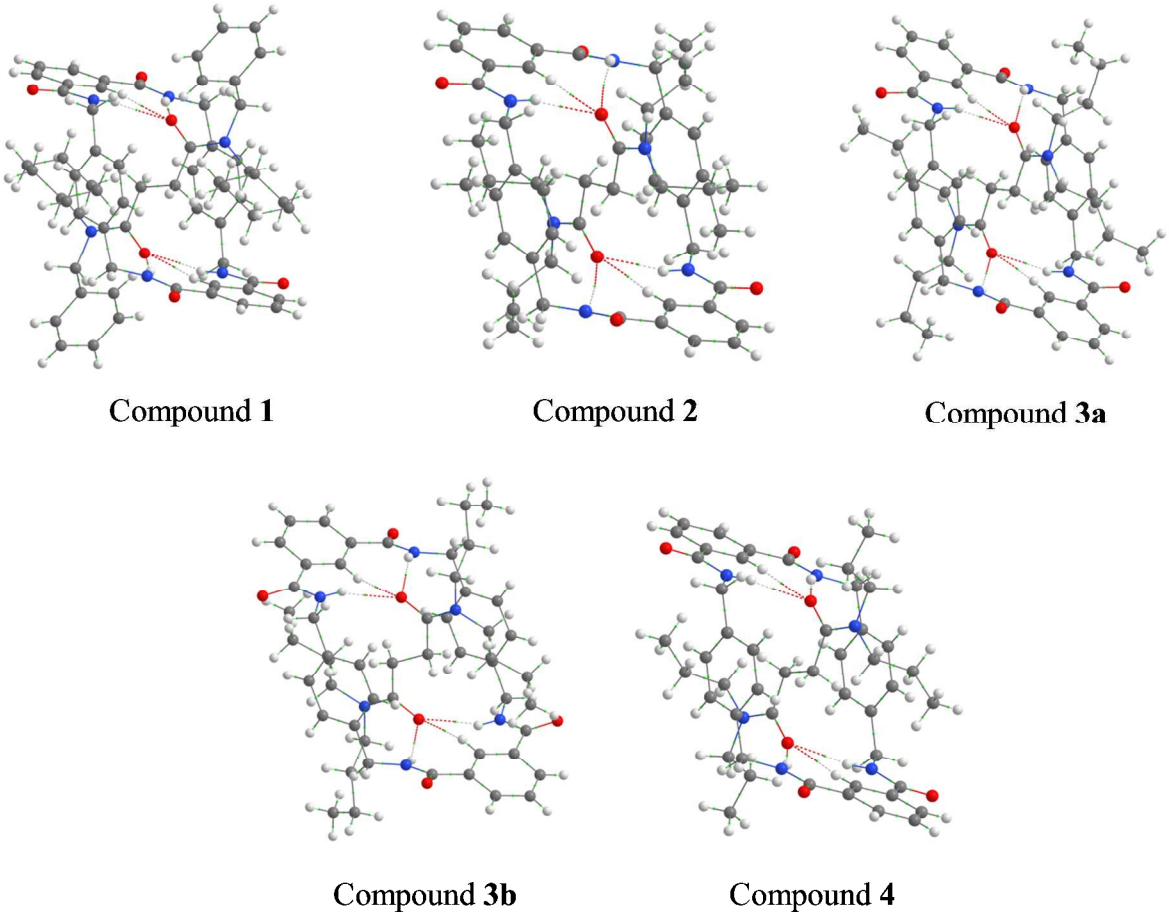

Figure 8. Trifurcated hydrogen bonds in compounds **1–4**.

More properties relevant to all of the hydrogen bondings are given in the Supporting Information (Table S2-S6). These data let us discuss whether these hydrogen bonding fit the three main topological criteria established by Koch and Popelier.[52] A first necessary condition to confirm the presence of a hydrogen bond is the observation of a BCP between the hydrogen atom and the acceptor atom. The second necessary condition involves a local property, namely, the charge density evaluated at the BCP, referred to as ρ. The values were in the range of 0.002–0.034 au, and typically are smaller than those found for a covalent bond. The third necessary criterion focuses on another local property, namely, the Laplacian of the charge density evaluated at the BCP, referred to as $\nabla^2\rho$. It is crucial that $\nabla^2\rho$ be positive, but also that the values

range from 0.024 to 0.139 a.u (allowing for small differences in basis set). Thus, all the hydrogen bonding in compounds **1**–**4** follow criteria established by Koch and Popelier.

After the hydrogen bonds, the most important interactions are the CH···π type. These interactions can be classified as: (*i*) two sets of interactions between the succinamide station and the 1,4-phenylenediamine ring (with energies in the range of -2.72 to -0.98 kcal.mol^{-1} for each interaction — see Figure 9); (*ii*) interactions between the stoppers' alkyl chains and the isophthalamide ring — four sets of interactions for compound **1** (with energies in the range of -2.33 to -0.93 kcal mol^{-1} for each interaction), three sets of interactions for compound **2** (with energies in the range of -2.34 to - 0.82 kcal mol^{-1} for each interaction), and two sets of interactions for compounds **3a** and **3b** (with energy values in the range of -2.28 to - 1.71 kcal mol^{-1} for each interaction), one set of interactions for compound **4** (with -1.47 kcal mol^{-1} for each interaction) (Figure 10); and (*iii*) interactions between the stoppers' alkyl chains and the phenylenediamine ring — one set of interactions for compounds **1** and **2** (-1.53 and -1.16, respectively) (Figure 11). It is very important to note that these interactions do not occur in compounds **3a** and **3b**. The total energies of the CH···π interactions were -27.34, -18.88, -17.10, -14.86, and -11.62 kcal mol^{-1} for compounds **1**–**4**, respectively. Thus, we can say that the larger and more branched the alkyl chain of the stoppers, the greater the number of CH···π interaction paths between the thread and the macrocycle, which again confirms the data previously discussed in Table 2.

It is worth mentioning that C-H···π interactions are also unique if they refer to the typical hydrogen bonds. According to Pauling's definition of hydrogen bonding, [53] such an interaction is formed if the covalently bound hydrogen atom (X-H bond, in which X is an electronegative atom) interacts with the other electronegative centre (designated as Y). In the case of C-H···π

interactions, the π-electrons act as acceptors (Y). A later statistical study, based on the Cambridge Structural Database, [54] definitively proved that C-H···π interactions are attributed to hydrogen bonds. There are numerous studies stating that C-H···π interactions may be classified as hydrogen bonds with multicentre proton acceptors. [55]

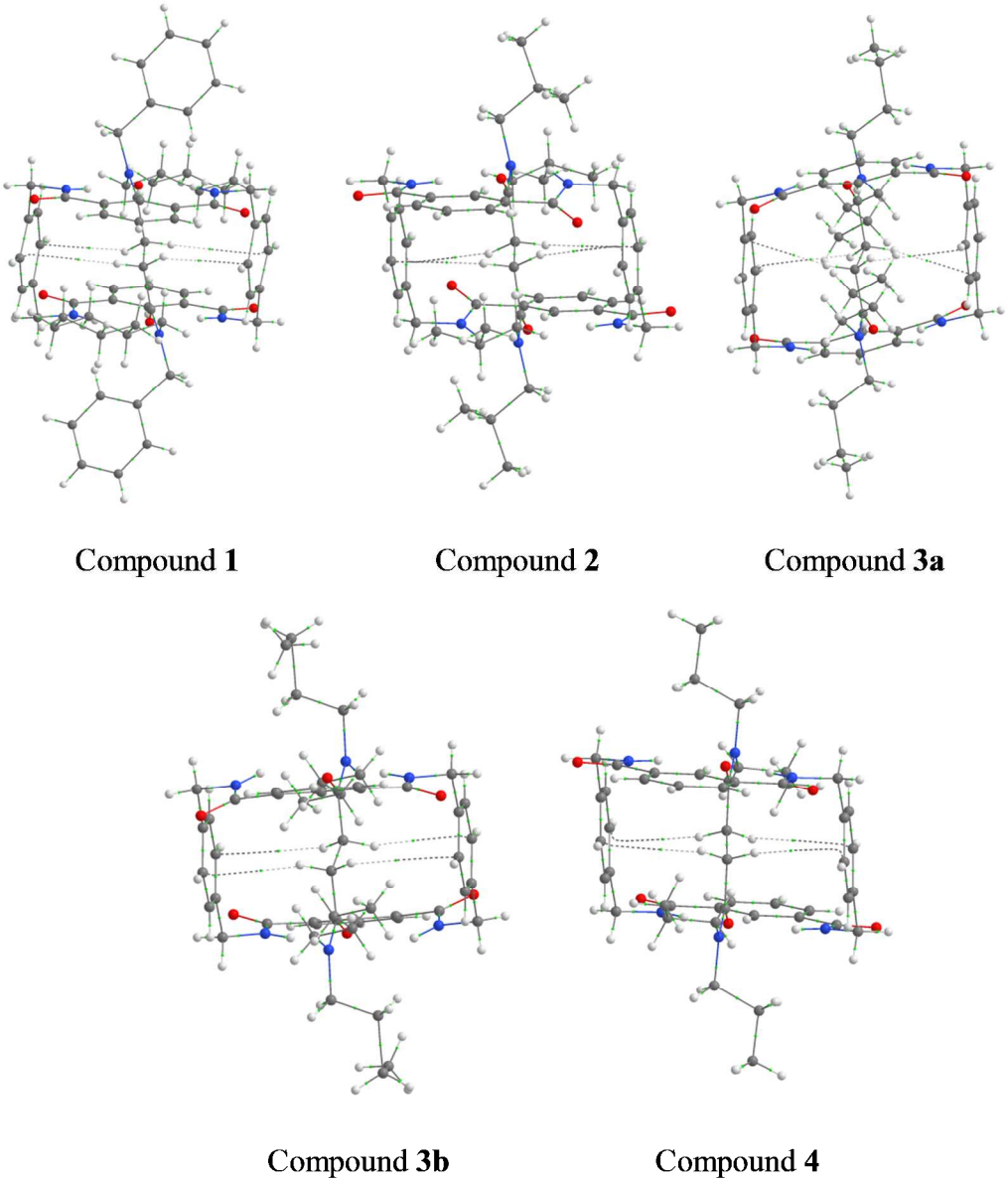

Figure 9. CH···π interactions, between the succinamide station and the 1,4-phenylenediamine ring, for all of the compounds.

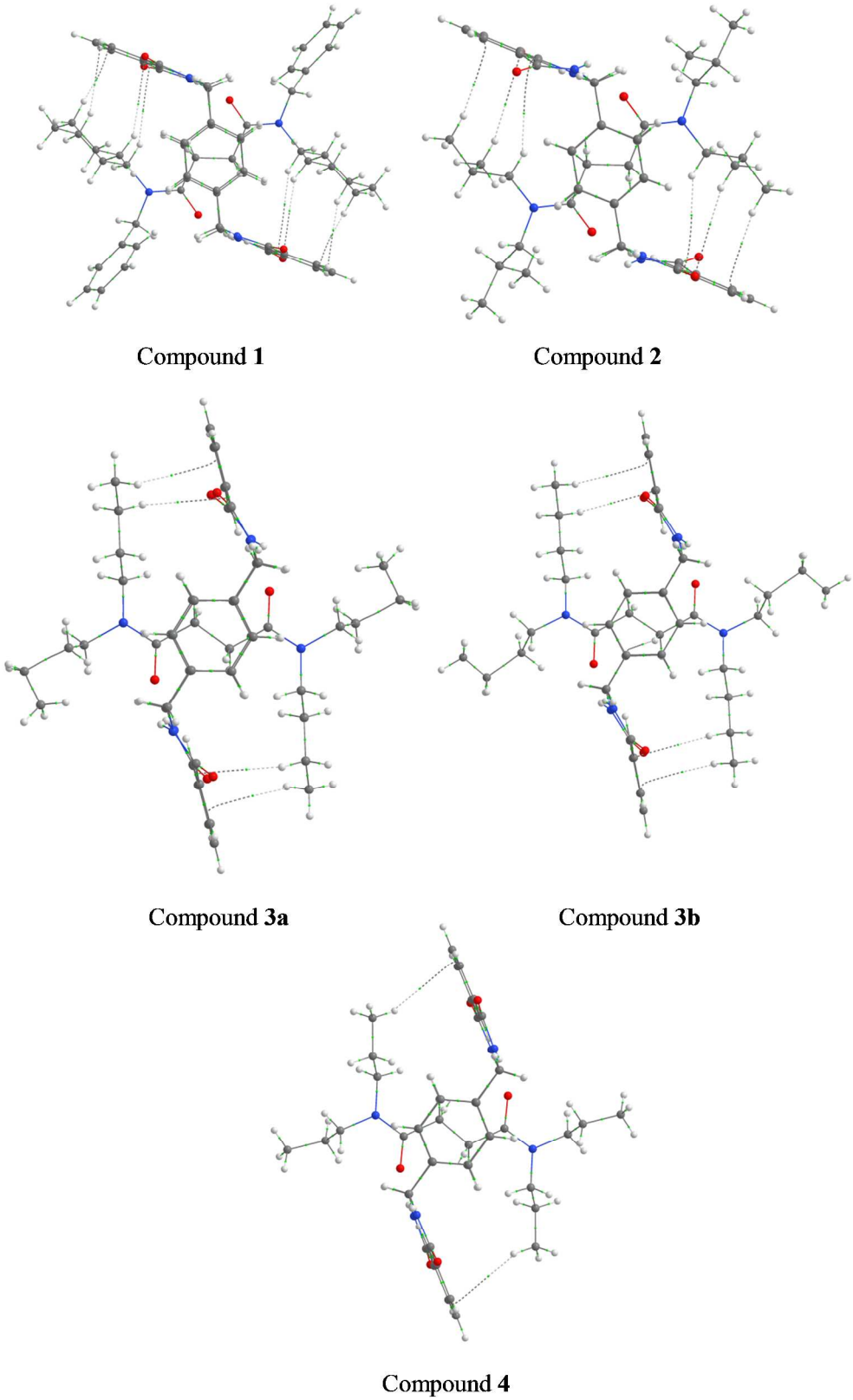

Figure 10. CH···π interactions, between the stoppers' alkyl chains and the isophthalamide ring.

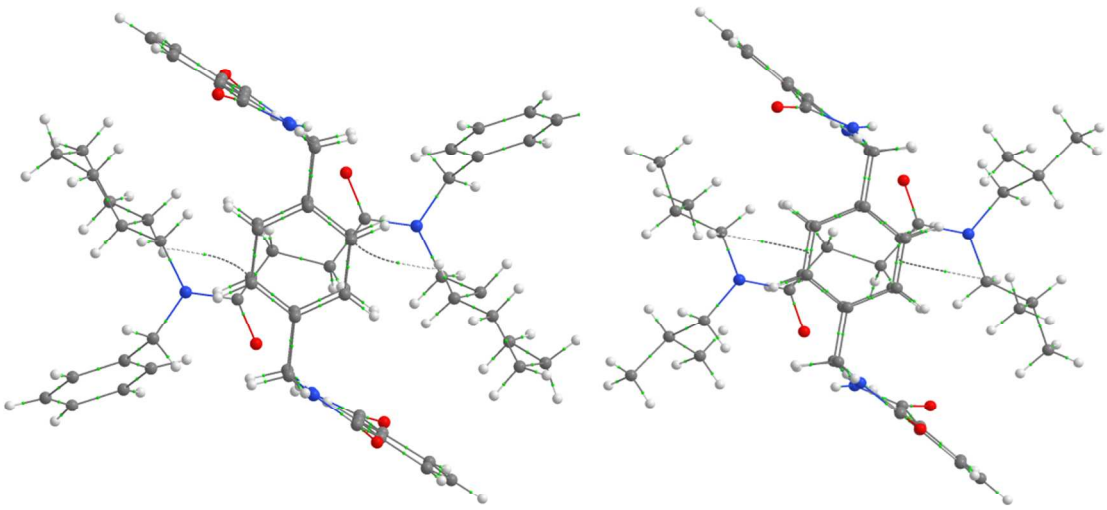

Compound **1** Compound **2**

Figure 11. CH···π interactions, between the stoppers' alkyl chains and the phenylenediamine ring.

Finally, H···H interactions were found in all of the compounds, and they appear as weak interactions — with energies in the range of -1.77 to -0.43 kcal mol^{-1} — that occur between the stoppers and the macrocycle. Added together, all these H···H interactions represent -4.72, -5.64, -2.88, -7.17, and -5.80 kcal mol^{-1}, for compounds **1**–**4**, respectively (Figure 12).

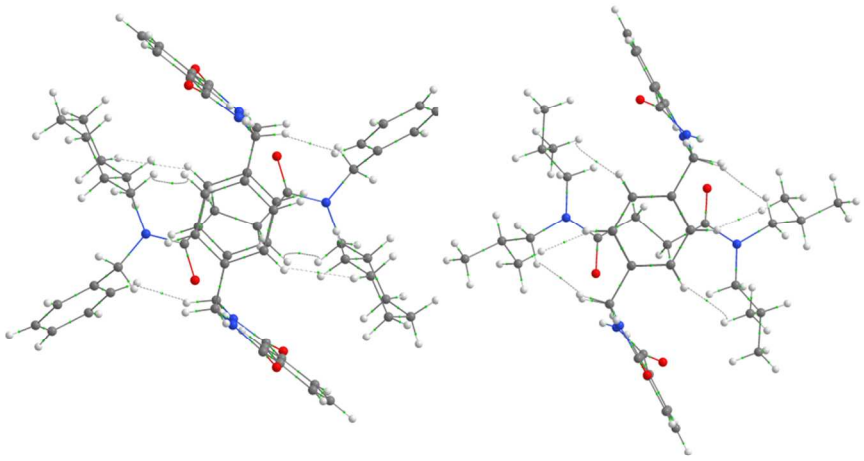

Compound **1** Compound **2**

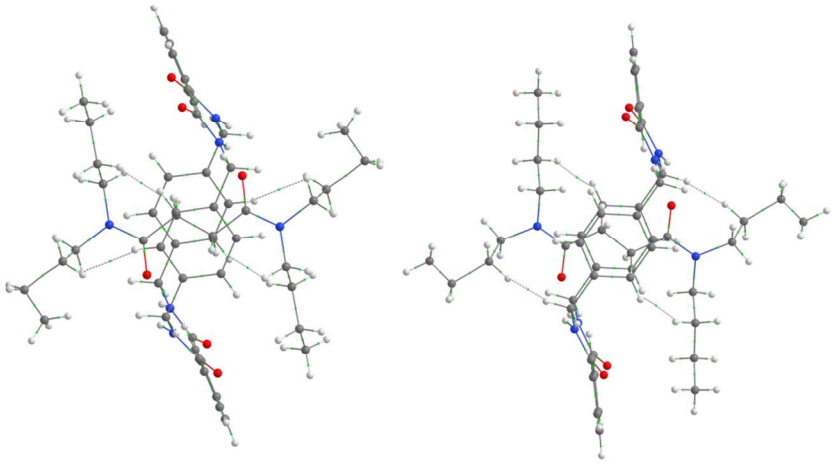

Compound **3a** Compound **3b**

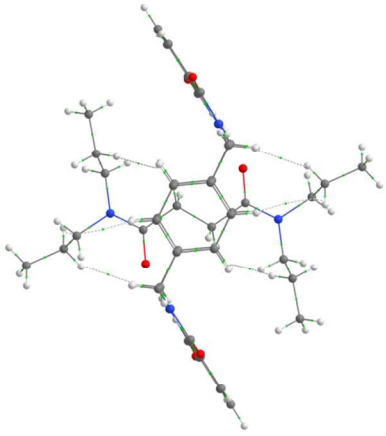

Compound **4**

Figure 12. H¨¨H interactions, between the stoppers and macrocycles, for all of the compounds.

Compounds **3a** and **4** show only these intramolecular interactions. On the other hand, there were π_{hole}···π interactions — between the carbon carbonyl of the thread station and the 1,4-phenylenediamine ring — for compounds **1**, **2**, and **3b**, with energy values of -1.61, -1.47, and -1.12 kcal mol^{-1} , respectively (Figure 13).

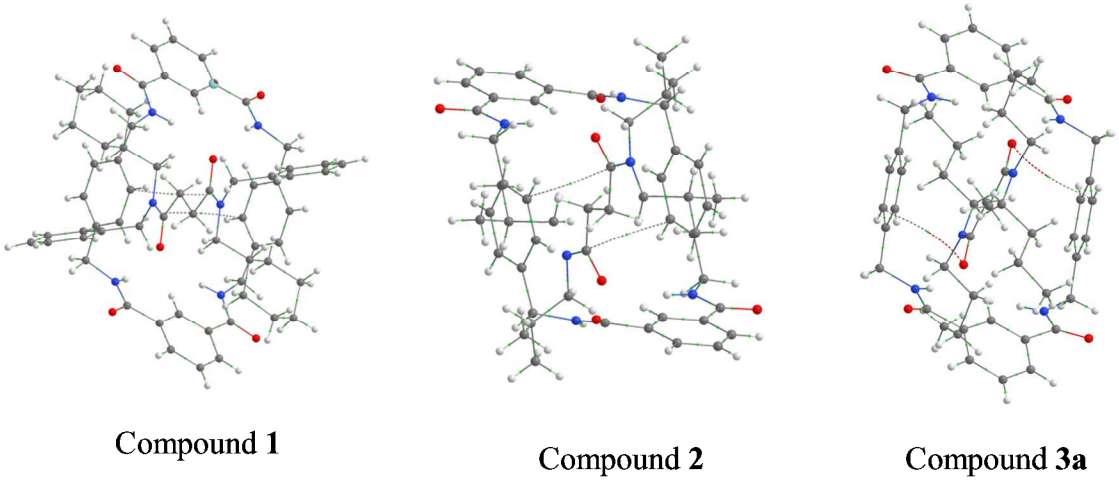

Figure 13. π_{hole}···π interaction , between the succinamide station and macrocycles.

An important feature of the bonding interactions in terms of the AIM theory is the ellipticity (ε) values. The ellipticity was suggested by Bader et al. for the quantitative description of the electron density deviation from the cylindrical symmetry in the CP of the (3, -1) type [56]. In fact, the value of ε characterizes the cycle susceptibility to opening. In this sense, the contacts with high ellipticity are potentially unstable. In such cases there is a high probability of bifurcation catastrophe, i.e. fusion of bond and ring critical points (CP (3, -1) and (3 + 1),respectively), which leads to unstable degenerate CP occurrence ($w < 3$).[57,58] Thus, the analysis of the ellipticity (ε) values for compounds **1-4** allows (see Supporting Information, Table S2-S6) to predicted that some CH···π interactions in all compounds and one set of H···H interactions in the compound **3b** are unstable, but can be experimentally determined. However these interactions

was not neglected because these was proven using NCIPLOT program[38] (for NCI data see Supporting Information, Figures S8-S12), furthermore manifestations of these interactions in the compounds studied will be investigated by NMR ^{1}H experiments, described below. For these reasons the energies of these interactions were considered.

In this sense, in order to provide an insight into the intramolecular interactions in solution, ^{1}H NMR experiments were used. The experiments were done in $CDCl_3$, and they showed the large temperature-dependent changes in chemical shifts for some of the signals that are involved in CH···π interactions and hydrogen bonding. In particular, the downfield shift of the amide proton signal is characteristic of hydrogen bonding interactions between the amide groups, when atoms that are involved in hydrogen bonds have the effect of decreasing the electron density around the hydrogen atom, which leads to deshielding. On the other hand, the upfield shift of the methylene signals is characteristic of CH···π interactions and is due to the proximity at the phenyl ring. The upfield shift is probably a result of the anisotropic effect due to the aromatic ring's proximity.

Thus, in order to prove that the intramolecular interactions observed in the solid state can also be verified in solution, all of the compounds were subjected to variable temperature (VT) NMR experiments in $CDCl_3$ solutions. The concentration of the samples was fixed (0.04 M) in all of the experiments, within a range of 238–323 K, with increments of 5 K. For the macrocycle, the signals that were analysed were: (*i*) the NH amide group (H^D, Figure 14); and (*ii*) the CH group belonging to isophthalamide (H^C, Figure 14), both of which are involved in N-H···O and C-H···O hydrogen bonds. For the thread, the signals that were analysed were: (*i*) the methyl group belonging to the succinamide portion of the thread (H^a, Figure 14); and (*ii*) the methyl group belonging to the stoppers (H^d for compounds **1**, **3**, and **4**; and H^e for compound **2** — see Figure 14), both of which are involved in CH···π interactions with the phenyl units of the macrocycle. It

is worth to mentioning that for compound **1**, only conformer **1a** (*Z*,*Z*) was accompanied by VT-NMR experiments, due to this conformer being studied in solid state.

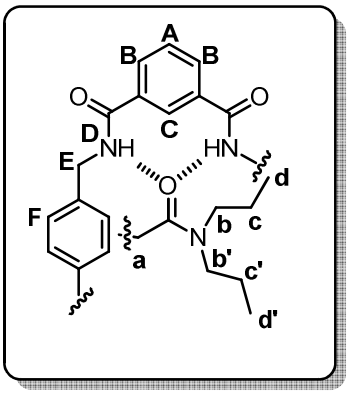

Figure 14. Nomenclature used in the ^{1}H NMR spectra, with compound **4** as an example.

The ^{1}H NMR chemical shifts of compounds **1**–**4** are shown in the Table S8, together with the reduced temperature coefficients ($\Delta\delta/\Delta T$), derived from the VT-NMR, in ppb·K^{-1}. The temperature's dependence on the amide proton's NMR chemical shift has been widely used a standard parameter in the characterization of peptide behaviour in solution, [59,60] but this is the first time that this treatment has been described for Leigh-type rotaxanes. The data showed the chemical shift's high dependence on the temperature, so that the hydrogens involved in the hydrogen bonding shield with the increasing temperature, while the hydrogens involved in CH···π interactions deshielded with the increasing temperature. This occurs because the temperature increase leads to the pirouetting movement of [2]rotaxane, which occurs with the breaking of intramolecular interactions between the thread and the macrocycle.

Of all the compounds studied, the NH···O type hydrogen bond is more dependent on the temperature than the CH···O interactions, while the CH···π interactions between the succinamide station are more dependent on the temperature than the interactions between the stoppers. It is known that the $\Delta\delta/\Delta T$ values of the NH hydrogen are directly related to the proton mobility.[61]

Thus, Figure 15 shows the dependence of the reduced temperature coefficients ($\Delta\delta/\Delta T$) on the energy of the interactions for compounds **1**–**4**. The data are consistent and demonstrate that the strongest hydrogen bonds show a greater change in chemical shift with the VT-NMR experiments (G_{AI}= 7.21($\Delta\delta/\Delta T$) - 6.69; r = 0.935).

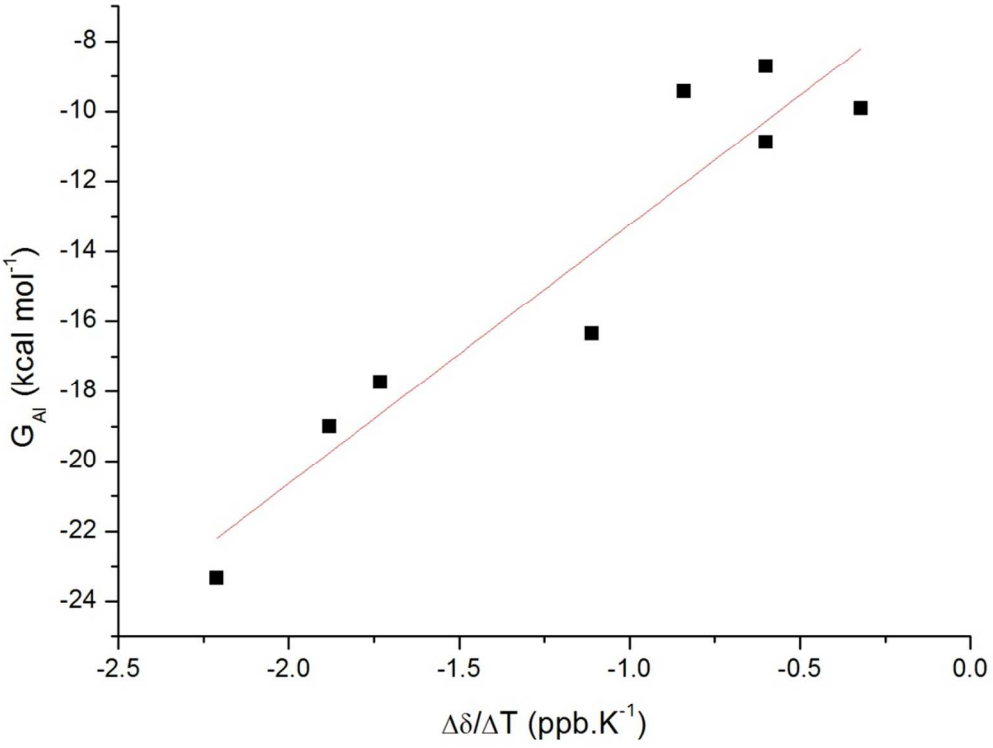

Figure 15. Correlation between the hydrogen bonding energy and the reduced temperature coefficients for compounds **1**–**4**.

The second relevant aspect is that the VT-NMR experiments provide important information about the pirouetting process in [2]rotaxanes. This study enabled the determination of the energy barriers ($\Delta G^{\neq}$) for the rotation of the macrocycle, through the monitoring of the methylene hydrogens of the macrocycle. The cooling leads to the freezing of the pirouetting process and, consequently, the methylene hydrogens are resolved into two distinct signals (H_E and $H_{E'}$). In

order to increase the temperature, these peaks coalesce into one broad peak, which indicates that the exchange process is fast on the NMR time scale. The energy barrier for the compounds can be calculated from the coalescence temperature and the limiting chemical shift difference of the methylene hydrogens (Table 3) (For more informaton see Supporting Information, Figure S15).

From the results shown in Table 3, the high values of the energy barriers — calculated for the macrocycle pirouetting process in the [2]rotaxanes **1** containing cyclohexylmethyl and benzyl stoppers — should be noted. These values are higher than those calculated for the [2]rotaxanes **2**–**4**, which clearly differentiates the effect of the stoppers in the pirouetting movement. In turn, compound **3** — which is equipped with longer alkyl chains (butyl) — had the second highest rotational barrier value of all the compounds studied. Finally, lower rotational barrier values were observed for compounds **2** and **4** — compound **2** probably had lower values due to the fact that it has weaker hydrogen bonds than compound **4** (see Table 2).

In short, we can say that the higher the energy of the intramolecular interactions ($G_{Mcy\cdots Thr}$), the greater the coalescence temperature and, therefore, the greater the energy barrier ($\Delta G^{\neq}$) for the rotation of the macrocycle (for the correlation between coalescence temperature and rotational energy barrier see Figure S14 in the Supporting Information; $\Delta G^{\neq}=0.0383T_C + 1.6644$; r= 0.973). Figure 16 shows the dependence of the energy barrier ($\Delta G^{\neq}$) on the intramolecular interaction energy ($G_{Mcy\cdots Thr}$) for compounds **1–4** ($\Delta G^{\neq}=-0.1349G_{Mcy\cdots Thr}+6.4706$; r= 0.907). The data obtained are consistent and demonstrate that more energy is required to break all the intramolecular interactions and for the macrocycle to rotate freely around the thread, due to there being more interactions between the thread and macrocycle.

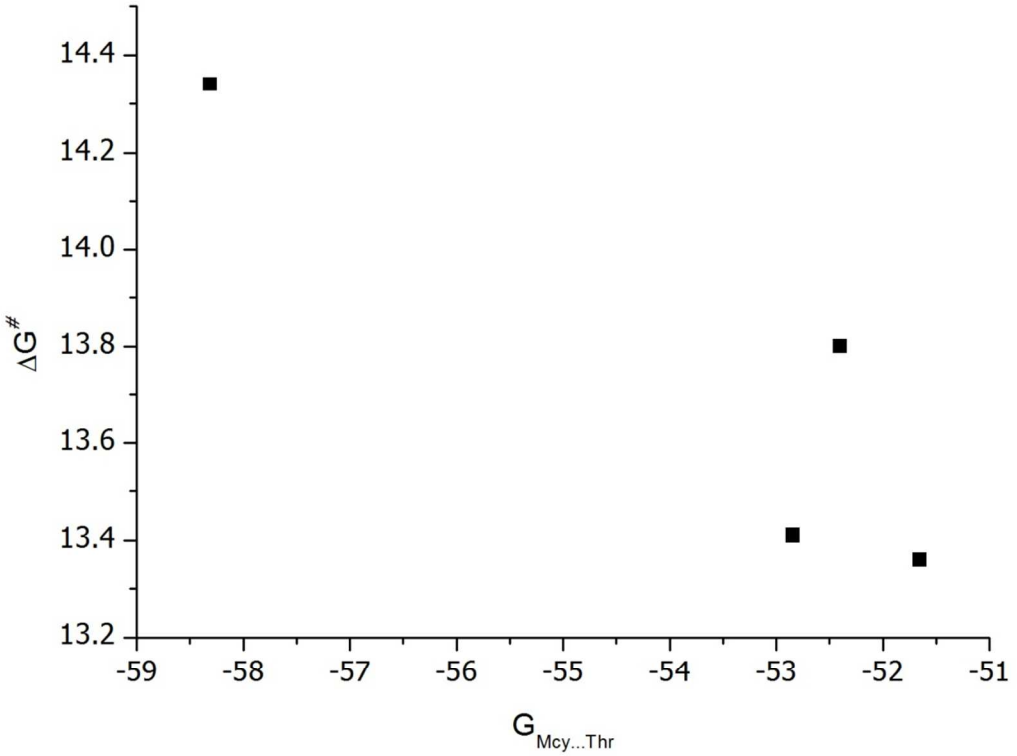

Figure 16. Correlation between the rotational energy barriers ($\Delta G^{\neq}$) and the intramolecular interactions ($G_{Mcy\cdots Thr}$) for compounds **1–4**.

With these data in hand, it is clear that the greater the number of stoppers, the greater the possibility of CH···π interactions and, consequently, the higher the values of the rotational barrier. Another fact that supports this theory is the observation of kinetic parameters for macrocycle pirouetting, obtained for conformers **1b** and **1c** observed in the compounds in solution. Conformer **1b** has the possibility of CH···π interactions with only one cyclohexyl stopper, and it has intermediate rotational barrier values compared to conformer **1a**, which has CH···π interactions with both cyclohexyl stoppers. Conformer **1c** does not have the possibility of CH···π interactions between the cyclohexyl stoppers and the macrocycle and, therefore, it has the lowest amount of pirouetting energy.

It is important to note that for the temperatures at which the VT-NMR experiments were performed (238–323 K), the percentage of conformers observed for compound **1** remained the same, indicating that much energy is required to convert one conformer into another.

Also, when trying to identify the stablest conformer of compounds **1a**–**c**, theoretical calculations were performed to determine the single crystal's point structure and energy minimization, using the Gaussian09 software package. [33] The calculations were performed at a ωB97X -D/cc-pVDZ level of theory, and the results confirm that conformer **1a** is the stablest among the conformers formed — conformers **1b** and **1c** are 1.2 and 1.5 kcal mol $^{-1}$, respectively, less stable than conformer **1a**.

Table 3. Kinetic parameters for macrocycle pirouetting, obtained from the temperature-dependent ^{1}H NMR spectra of the [2]rotaxanes **1**–**4**.

Compound	δH_E; $\delta H_{E'}$	$\Delta\nu$[a]	k_c[b]	T_c (K)[c]	$\Delta G^{\neq}$[d]
1a[e]	5.24; 3.13	884.18	1876.7	328	14.34
1b[e]	5.44; 3.66	712.16	1583.77	296	12.98
1b[e]	5.02; 3.44	632.14	1406.32	296	13.04
1c[e]	5.08; 3.85	492.11	1095.57	278	12.36
2[e]	5.42; 3.69	692.16	1539.42	305	13.41
3[e]	5.38; 3.71	668.15	1486.13	313	13.80
4[f]	5.39; 3.76	978	2171.56	313	13.36

[a] $\Delta\nu$ is the separation (in Hz) between the resonance peaks of the axial (H_E) and equatorial ($H_{E'}$) benzylic hydrogens in the slow exchange regime.

[b] k_c is the rate of exchange in s^{-1}.

[c] T_c is the coalescence temperature in K.

[d] $\Delta G^{\neq}$ is the energy barrier in kcal mol^{-1} (free energy of activation) of the ring rotation process.

[e] VT-NMR experiments (400 MHz) were performed using $CDCl_3$ (low temperature) or $C_2D_2Cl_4$ (high temperature) in the samples.

[f] VT-NMR experiments (600 MHz) were performed using $CDCl_3$ in the samples.

Conclusion

In summary, in this paper, an in-depth study concerning the structure of four Leigh-type [2]rotaxanes is reported. The compounds have small differences in stoppers, which directly influences the interactions between supramolecular components.

The hydrogen bonding is very important in [2]rotaxanes containing benzylic amide macrocycles, but there are others interactions (e.g., C-H···π, π_{hole}···π, and H···H) that have rarely been described in the literature for [2]rotaxanes. All the interactions were qualified and quantified using theoretical calculations (DFT and QTAIM analysis) in solid state and VT-NMR experiments in liquid state.

It was observed that the greater the contact surface between the thread and the macrocycle, the greater the interaction energy obtained and, therefore, the higher the calculated energy barriers for the macrocycle pirouetting process. Thus, compound **1** — which had different conformers in solution — was of fundamental importance in reaching these conclusions, demonstrating the importance of the C-H···π interactions in the pirouetting process.

Finally, the present work offers a new way of understanding all the interactions between the macrocycle and the thread, based on theoretical data, which are very important for future designs so that [2]rotaxanes can shuttle and/or rotate in the solid state. And we believe such features create a new expectation for the elaboration of more complex molecular machines for analyzing intramolecular interactions.

ASSOCIATED CONTENT

Supporting Information

^{1}H, ^{13}C, LCMS and HRMS of compounds synthesized, micrographics of the crystals, atomic coordinates used in theoretical calculations for conformers **1a-c**, QTAIM and NCI data for all compounds, contact area between the thread and the macrocycle, NMR Chemical Shift Temperature Dependences ($ppb.K^{-1}$) for all compounds in $CDC1_3$ and Variable temperature ^{1}H NMR spectra of the [2]rotaxanes. This material is available free of charge via the Internet at http://pubs.acs.org.

AUTHOR INFORMATION

Corresponding Author

* mmartins@base.ufsm.br

ACKNOWLEDGMENT

The authors are thankful for the financial support from: the Conselho Nacional de Desenvolvimento Científico e Tecnológico (CNPq)—Universal/Proc. 475556/2012-7 and 474895-2013-0; Fundação de Amparo à Pesquisa do Estado do Rio Grande do Sul; Coordenação de Aperfeiçoamento de Pessoal de Nível Superior (CAPES/PROEX); MINECO (CTQ2014-56887-P) with joint financing by FEDER Funds from the European Union, and Fundacion Seneca-CARM (Project 19240/PI/14).The fellowships from CNPq (M.A.P.M., N.Z., H.G.B. and C.P.F.) and the fellowships from CAPES (A.R.M and L.V.R.) are also acknowledged.

REFERENCES

(1) Amabilino, D. B.; Stoddart, J. F. *Chem. Rev.* **1995**, *95*, 2725–2828.

(2) Dietrich-Buchecker, C. O.; Sauvage, J. P. *Chem. Rev.* **1987**, *87*, 795–810.

(3) Sauvage, J.-P.; Dietrich-Buchecker, C. O. *Molecular Catenanes, Rotaxanes and Knots: A Journey Through the World of Molecular Topology*; Wiley-VCH, W., Ed.; 1999.

(4) Stoddart, J. F. *Chem. Soc. Rev.* **2009**, *38*, 1802.

(5) Bruns, C. J.; Stoddart, J. F. *The Nature of the Mechanical Bond*; John Wiley & Sons, Inc.: Hoboken, NJ, USA, 2016.

(6) Sauvage, J.-P.; Gaspard, P. *From Non-Covalent Assemblies to Molecular Machines*; Sauvage, J.-P., Gaspard, P., Eds.; Wiley-VCH Verlag GmbH & Co. KGaA: Weinheim, Germany, 2010.

(7) Berná, J.; Alajarín, M.; Martínez-Espín, J. S.; Buriol, L.; Martins, M. A. P.; Orenes, R.-Á. *Chem. Commun.* **2012**, *48*, 5677.

(8) Martinez-Cuezva, A.; Rodrigues, L. V.; Navarro, C.; Carro-Guillen, F.; Buriol, L.; Frizzo, C. P.; Martins, M. A. P.; Alajarin, M.; Berna, J. *J. Org. Chem.* **2015**, *80*, 10049–10059.

(9) Collins, C. G.; Peck, E. M.; Kramer, P. J.; Smith, B. D. *Chem. Sci.* **2013**, *4*, 2557–2563.

(10) Martinez-Cuezva, A.; Carro-Guillen, F.; Pastor, A.; Marin-Luna, M.; Orenes, R.; Alajarin, M.; Berna, J. *ChemPhysChem* **2016**, *17*, 1920–1926.

(11) Barendt, T. A.; Robinson, S. W.; Beer, P. D. *Chem. Sci.* **2016**, *7*, 5171–5180.

(12) Jagesar, D. C.; Wiering, P. G.; Kay, E. R.; Leigh, D. A.; Brouwer, A. M. *ChemPhysChem* **2016**, *17*, 1902–1912.

(13) Biscarini, F.; Cavallini, M.; Leigh, D. A.; León, S.; Teat, S. J.; Wong, J. K. Y.; Zerbetto, F. *J. Am. Chem. Soc.* **2002**, *124*, 225–233.

(14) Pikulska, A.; Pecul, M. *J. Phys. Chem. A* **2011**, *115*, 10795–10800.

(15) Malberg, F.; Brandenburg, J. G.; Reckien, W.; Hollóczki, O.; Grimme, S.; Kirchner, B. *Beilstein J. Org. Chem.* **2014**, *10*, 1299–1307.

(16) Lehn, J.-M. *Chem. Soc. Rev.* **2007**, *36*, 151–160.

(17) Marlin, D. S.; González Cabrera, D.; Leigh, D. A.; Slawin, A. M. Z. *Angew. Chemie* **2006**, *118*, 83–89.

(18) Hannam, J. S.; Lacy, S. M.; Leigh, D. A.; Saiz, C. G.; Slawin, A. M. Z.; Stitchell, S. G. *Angew. Chemie - Int. Ed.* **2004**, *43*, 3260–3264.

(19) Baumes, J. M.; Murgu, I.; Oliver, A.; Smith, B. D. *Org. Lett.* **2010**, *12*, 4980–4983.

(20) Glink, P. T.; Oliva, A. I.; Stoddart, J. F.; White, A. J. P.; Williams, D. J. *Angew. Chemie Int. Ed.* **2001**, *113*, 1922–1927.

(21) Ahmed, R.; Altieri, A.; D'Souza, D. M.; Leigh, D. A.; Mullen, K. M.; Papmeyer, M.; Slawin, A. M. Z.; Wong, J. K. Y.; Woollins, J. D.; Ahmed, S. I.; Based, P.; Rotaxanes, S.; Ahmed, R.; Altieri, A.; Souza, D. M. D.; Leigh, D. A.; Mullen, K. M.; Slawin, A. M. Z.; Wong, J. K. Y.; Woollins, J. D. *J. Am. Chem. Soc. 2011,* **2011**, *133*, 12304–12310.

(22) Bader, R. F. W. *Acc. Chem. Res.* **1985**, *18*, 9–15.

(23) Bader, R. F. W. *Chem. Rev.* **1991**, *91*, 893–928.

(24) Bader, R. F. W. *Atoms in Molecules. A Quantum Theory*; A Clarendon Press Publication, Ed.; 1990.

(25) Popelier, P. *Atoms in Molecules. An Introduction*; Prentice Hall, Ed.; New York, 2000.

(26) Nador, F.; Moglie, Y.; Ciolino, A.; Pierini, A.; Dorn, V.; Yus, M.; Alonso, F.; Radivoy, G. *Tetrahedron Lett.* **2012**, *53*, 3156–3160.

(27) Cho, B. T.; Kang, S. K. *Tetrahedron* **2005**, *61*, 5725–5734.

(28) Deng, J.; Mo, L.-P.; Zhao, F.-Y.; Hou, L.-L.; Yang, L.; Zhang, Z.-H. *Green Chem.* **2011**, *13*, 2576.

(29) Bruker, APEX2 (Version 2.1), COSMO (Version 1.56), BIS (Version 2.0.1.9) SAINT (Version 7.3A) and SADABS (Version 2004/1) and XPREP (Version 2005/4), Bruker AXS Inc., Madison, Wisconsin, USA, 2006. .

(30) Sheldrick, G. M. *Acta Crystallogr. Sect. A Found. Crystallogr.* **2008**, *64*, 112–122.

(31) Coppens, P.; Leiserowitz, L.; Rabinovich, D. *Acta Crystallogr.* **1965**, *18*, 1035–1038.

(32) Farrugia, L. J. ; J. Appl. Cryst. 32, 837-838.

(33) Frisch, E.; Frisch, M. J.; Trucks, G. W.; Schlegel, H. B.; Scuseria, G. E.; Robb, M. A.; Cheeseman, J. R.; Montgomery, Jr., J. A.; Vreven, T.; Kudin, K. N.; Buran, J. C.; Millam, J. M.; Iyengar, S. S.; Tomasi, J.; Barone, V.; Mennuncci, B.; Cossi, M.; Scalmani, G.; Rega, N.; Petersson, G. A.; Nakatsuji, H.; Hada, M.; Ehara, M.; Toyota, K.; Fukuda, R.; Hasegawa, J.; Ishida, M.; Nakajima, T.; Honda, Y.; Kitao, O.; Nakai, H.; Klene, M.; Li, X.; Knox, J. E.; Hratchian, H. P.; Cross, J. B.; Bakken, V.; Adamo, C.; Jaramillo, J.; Gomperts, R.; Stratmann, R. E.; Yazyev, O.; Austin, A. J.; Cammi, R.; Pomelli, C.; Ochterski, J. W.; Ayala, P. Y.; Morokuma, K.; Voth, G. A.; Salvador, P.; Dannenberg, J. J.; Zakrzewski, V. G.; Dapprich, S.; Daniels, A. D.; Strain, M. C.; Farkas, O.; Malick, D. K.; Rabuck, A. D.; Raghavachari, K.; Foresman, J. B.; Ortiz, J. V.; Cui, Q.; Baboul, A. G.; Clifford, S.; Cioslowski, J.; Stefanov, B. B.; Liu, G.; Liashenko, A.; Piskorz, P.; Komaromi, I.; Martin, R. L.; Fox, D. J.; Keith, T.; Al-Laham, M. A.; Peng, C. Y.; Nanayakkara, A.; Challacombe, M.; Gill, P. M. W.; Johnson, B.; Chen, W.; Wong, M. W.; Gonzalez, C.; Pople, J. A. *Gaussian Pittsburgh, PA*. Gaussian, Inc.: Wallingford CT 2009.

(34) Boys, S. F.; Bernardi, F. *Mol. Phys.* **1970**, *19*, 553–566.

(35) Keith, T. A. TK Gristmill Software,: Overland Park KS, USA, 2017.

(36) Ehresmann, B.; Martin, B.; Horn, A. H. C.; Clark, T. *J. Mol. Model.* **2003**, *9*, 342–347.

(37) Blatov, V., A.; Shevchenko, P. A. Samara State University, Ac. Pavlov St., 443011 Samara, Russia 2012.

(38) Johnson, E. R.; Keinan, S.; Mori-Sánchez, P.; Contreras-García, J.; Cohen, A. J.; Yang, W. *J. Am. Chem. Soc.* **2010**, *132*, 6498–6506.

(39) Humphrey, W.; Dalke, A.; Schulten, K. *J. Mol. Graph.* **1996**, *14*, 33–38.

(40) Leigh, D. A.; Murphy, A.; Smart, J. P.; Slawin, A. M. Z. *Angew. Chem. Int. Ed. Engl.* **1997**, *1*, 728–732.

(41) Gatti, F. G.; Leigh, D. A.; Nepogodiev, S. A.; Slawin, A. M. Z.; Teat, S. J.; Wong, J. K. Y. *J. Am. Chem. Soc.* **2001**, *123*, 5983–5989.

(42) Clegg, W.; Gimenez-Saiz, C.; Leigh, D. A.; Murphy, A.; Slawin, A. M. Z.; Teat, S. J. *J. Am. Chem. Soc.* **1999**, *121*, 4124–4129.

(43) Martinez-Cuezva, A.; Berna, J.; Orenes, R. A.; Pastor, A.; Alajarin, M. *Angew. Chemie - Int. Ed.* **2014**, *53*, 6762–6767.

(44) Brancato, G.; Coutrot, F.; Leigh, D. A.; Murphy, A.; Wong, J. K. Y.; Zerbetto, F. *Proc. Natl. Acad. Sci. U. S. A.* **2002**, *99*, 4967–4971.

(45) Brouwer, A. M.; Frochot, C.; Gatti, F. G.; Leigh, D. A.; Mottier, L.; Polucci, F.; Roffia, S.; Wurpel, G. W. H. *Science* **2001**, *291*, 2124–2128.

(46) Martins, M. A. P.; Hörner, M.; Beck, J.; Tier, A. Z.; Belladona, A. L.; Meyer, A. R.; Zanatta, N.; Bonacorso, H. G.; Frizzo, C. P. *CrystEngComm* **2016**, *18*, 3866–3876.

(47) Frizzo, C. P.; Bender, C. R.; Tier, A. Z.; Gindri, I. M.; Salbego, P. R. S.; Meyer, A. R.; Martins, M. A. P. *CrystEngComm* **2015**, *17*, 2996–3004.

(48) Martins, M. A. P.; Meyer, A. R.; Tier, A. Z.; Longhi, K.; Ducati, L. C.; Bonacorso, H. G.; Zanatta, N.; Frizzo, C. P. *CrystEngComm* **2015**, *17*, 7381–7391.

(49) Altieri, A.; Gatti, F. G.; Kay, E. R.; Leigh, D. A.; Martel, D.; Paolucci, F.; Slawin, A. M. Z.; Wong, J. K. Y. *J. Am. Chem. Soc.* **2003**, *125*, 8644–8654.

(50) Berná, J.; Leigh, D. a; Lubomska, M.; Mendoza, S. M.; Pérez, E. M.; Rudolf, P.; Teobaldi, G.; Zerbetto, F. *Nat. Mater.* **2005**, *4*, 704–710.

(51) Wurpel, G. W. H.; Brouwer, A. M.; van Stokkum, I. H. M.; Farran, A.; Leigh, D. A. *J. Am. Chem. Soc.* **2001**, *123*, 11327–11328.

(52) Koch, U.; Popelier, P. L. a. *J. Phys. Chem.* **1995**, *99*, 9747–9754.

(53) Pauling, L. *The Nature of the Chemical Bond and the Structure of Molecules and Crystals; An Introduction to Modern Structural Chemistry. (George Fisher Baker Non-Resident Lec)*, 3rd ed.; Cornell University Press: Ithaca: New York, 1960.

(54) Cambridge Crystallographic Data Centre. Cambridge,U.K. 2001.

(55) Grabowski, S. J. *J. Phys. Chem. A* **2007**, *111*, 3387–3393.

(56) Bader, R. F. W.; Slee, T. S.; Cremer, D.; Kraka, E. *J. Am. Chem. Soc.* **1983**, *105*, 5061–5068.

(57) Baryshnikov, G. V.; Minaev, B. F.; Minaeva, V. A.; Baryshnikova, A. T.; Pittelkow, M. *J. Mol. Struct.* **2012**, *1026*, 127–132.

(58) Baryshnikov, G. V.; Minaev, B. F.; Minaeva, V. A.; Nenajdenko, V. G. *J. Mol. Model.* **2013**, *19*, 4511–4519.

(59) Gellman, S. H.; Dado, G. P.; Liang, G. B.; Adams, B. R. *J. Am. Chem. Soc.* **1991**, *113*, 1164–1173.

(60) Urry, D. W.; Long, M. M. *CRC Crit. Rev. Biochem.* **1976**, *4*, 1–45.

(61) Martínez-Martínez, F. J.; Padilla-Martínez, I. I.; Brito, M. a.; Geniz, E. D.; Rojas, R. C.; Saavedra, J. B. R.; Höpfl, H.; Tlahuextl, M.; Contreras, R. *J. Chem. Soc. Perkin Trans. 2* **1998**, *2*, 401–406.

For Table of Contents Use Only

DFT and QTAIM analysis: Influence of intramolecular interactions on pirouetting movement in tetraalkylsuccinamide[2]rotaxanes

This work presents the study of all intramolecular interactions in different tetraalkylsuccinamide[2]rotaxanes. The QTAIM data allied with quantum mechanical calculations show hydrogen bonds, C–H···π, and, H···H interactions in these compounds. The intramolecular interactions shown to affect the pirouetting of the compounds studied. The higher energy of intramolecular interactions the higher the energy for the pirouetting movement.